IEEE Access
Multidisciplinary | Rapid Review | Open Access Journal

Received July 15, 2021, accepted August 21, 2021, date of publication August 24, 2021, date of current version September 2, 2021.

Digital Object Identifier 10.1109/ACCESS.2021.3107595

PMSG-Based Dual-Port Wind-Energy Conversion System With Reduced Converter Size

ALI BAKBAK[1], MERT ALTINTAS[1], MURAT AYAZ[2], HUSEYIN TAYYER CANSEVEN[3], MUTLU BOZTEPE[1], (Member, IEEE), OZKAN AKIN[1], AND ERKAN MESE[1], (Member, IEEE)

[1]Electrical and Electronics Engineering Department, Ege University, 35040 İzmir, Turkey
[2]Department of Electric and Energy, Kocaeli University, 41180 Kocaeli, Turkey
[3]Electrical and Electronics Engineering Department, Kütahya Dumlupınar University, 43000 Kütahya, Turkey

Corresponding author: Erkan Mese (erkan.mese@ege.edu.tr)

This work was supported by the Scientific and Technological Research Council of Turkey under Contract 117E785.

ABSTRACT In this study, a dual-port wind-energy conversion system has been proposed. A double-fed permanent-magnet synchronous generator (DFPMSG) forms the central part of the system, where the concentrated single-layer winding configuration of the generator enables electric and magnetic isolation between the ports. DFPMSG has two three-phase terminals out of the stator; one is connected directly to the grid, whereas the other is tied to the grid through a back-to-back converter. This study investigates design issues caused by the DFPMSG port with a direct grid connection. The unique design issues of the proposed system include determining the slot/pole combination using wind data and determining the minimum reactive power requirement for the port with a direct grid connection. Next, the load-sharing capability among the ports of the proposed system is presented through a detailed investigation of three schemes. Experimental work is presented for a 5-kW prototype DFPMSG system to illustrate the isolation among the ports, minimized reactive power demand on the port with direct grid connection, and load-sharing ability among the ports for different control schemes.

INDEX TERMS Double-fed machines, electric machine design, multi-port systems, permanent magnet synchronous generators, wind energy.

I. INTRODUCTION

Multi-port energy conversion systems have undergone extensive study recently in order to increase their fault-tolerance capability and to utilize the system for several simultaneous goals [1]–[4]. Although multi-port systems are generally preferred in applications where power converters and transformers are used together, it can also be applied to electrical machines. For example, in distribution systems, multi-port machine configurations provide isolation between winding sets, as well as additional redundancy [5]. Fault tolerance is also the driving motivation behind multi-port electric machines [6], [7]. For example, electric aircraft and micro-grid systems prioritize reliability in addition to high efficiency and compactness [3]. Furthermore, some applications focus on operating individual machines in different modes [8], [9]. In these modes, the machine may operate as a motor and generator, either simultaneously or independently.

The associate editor coordinating the review of this manuscript and approving it for publication was Yi Liu.

In the area of electric power generation, double-fed induction generators (DFIGs) are regarded as one of the earliest multiport electric machine applications in wind-energy conversion systems (WECS) [10]. These are preferred in WECS for their advantages, such as partial-scale power converter and low manufacturing cost [11]. The stator windings are connected to the grid directly, while the rotor is connected through a power converter. The rotor frequency, and thus rotor speed, is controlled by the power converter [12]. This concept supports a limited operation speed range (±30% synchronous speed) and is eligible for semi-variable speed operation. The main drawbacks of DFIG are its lower efficiency, gearbox requirement, and regular maintenance [13].

Brushless Double Fed Machines (BDFMs) were proposed at the turn of the last century and long before the era of power electronics for the operation of adjustable speed motors [14], [15]. Later, the concept was further developed and adapted for wind energy systems and several successful implementations have been reported [16], [17]. In [18] and [19], a variable speed stand-alone operation for a ship shaft generation was

reported, focusing on the control problems of the BDFM in such an application. As an alternative to the DFIG, BDFM can be considered as a remedy for brush and slip ring problems as these have been eliminated by a unique stator and rotor design. The reduced size of the converter is also considered an advantage inherited from the DFIG. The reactive power amplification is also a noticeable feature, although it has some limitations dictated by the speed range of the machine [17]. On the other hand, BDFMs are designed with relatively low pole pair numbers, which still requires the use of a gearbox before the generator. Moreover, inherent stability problems have been reported in the literature [16] and [17]. The design of BDFM is considered to be somewhat more challenging than conventional induction machines. The optimization of magnetic and electrical loading in the presence of winding sets with different number of poles in the stator and unique rotor cage structure are still challenging. As a result, 25% less output for the same active volume has been reported [17]. In a very recent design work [20], the pole number optimization has been well elaborated and documented with many aspects and performance metrics of BDFM.

Permanent-magnet synchronous generators (PMSGs), as an alternative to DFIGs and BDFMs, are becoming popular for their higher efficiency, higher torque density, high reliability, and wide operation speed range. Furthermore, gearboxes can be eliminated such that PMSGs with high pole numbers can operate efficiently at low speeds [21]. The stator is connected to the grid through a full-scale power converter, which can control the active and reactive power at all operating points to obtain a robust grid connection [22]. However, PMSGs have some disadvantages, such as their high initial cost due to their permanent magnets (PMs) and full-scale power converter requirement [23].

Double-fed PM synchronous generators (DFPMSGs) have become a popular research topic in the consideration of the aforementioned pros and cons of DFIGs, BDFMs, and PMSGs [24]–[30]. A concept study on DFPMSG has been performed in [24]. An analytical model is created for the simulation study of DFPMSG, and the operating conditions are discussed. The results are verified through simulation. In [25], a drive system for series-connected DFPMSM operating at a constant rotational speed is presented. It is mentioned that the machine design can be optimized to minimize losses. A control algorithm is developed to control the active and reactive power on the grid side. In [26]–[28], axial-flux PMSG with a double stator has been proposed for wind-turbine applications. Various control algorithms are performed on these machines. In addition to these works, a recent study of DFPMSG has been conducted by the authors [30]. In this study, the opportunities provided by the DFPMSG are investigated, and simulation studies are carried out for validation.

Owing to the increasing demand for reliable and cost-effective energy conversion systems, DFPMSGs are receiving more attention as multiport electrical machines with their

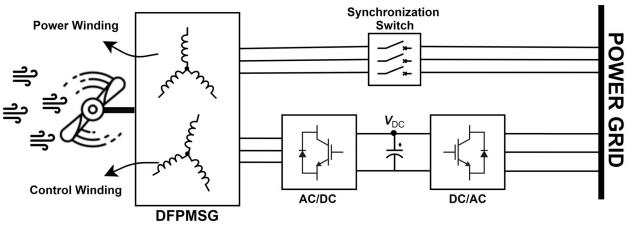

FIGURE 1. System diagram of the proposed concept.

isolated winding structure. Furthermore, the direct-drive ability inherited from the PMSG and the partial-scale power converter inherited from DFIG have become unique features of the proposed system. In this research, a dual-port WECS with DFPMSG is proposed. The DFPMSG includes two winding sets that are electrically and magnetically decoupled from each other. The winding sets are called power windings and control windings, as shown in Fig. 1. The power windings are connected to the grid directly, whereas, the control windings are connected to the grid via a back-to-back power converter. DFPMSG must rotate at a constant speed since the power windings are connected directly to the grid.

As far as the contributions of this paper are concerned, having a radial-flux, single air gap PMSG with an appropriately wound isolated winding set can be considered as the first contribution to achieve dual power generation channels. Presenting the concept at the system level and solidifying the design requirements for the given wind site data to maximize efficiency is the second contribution. Finally, load sharing scenarios within a wind energy system and proposed control schemes are the third contribution of the proposed system. The proposed concept is detailed in Section II. Subsequently, the design requirements of DFPMSG are determined and explained analytically and verified through finite-element analysis. The system-control algorithms to manage power flow are discussed in Section IV. Finally, the control algorithms and design specifications are tested on a prototype DFPMSG, and the results are presented.

II. PROPOSED CONCEPT

The proposed generator contains two magnetically and electrically decoupled winding sets, named control and power. The control winding is connected to the grid via a back-to-back (AC/DC-to-DC/AC) converter allowing bidirectional energy flow, whereas the power winding is directly connected to the grid. The start-up process, synchronization, and maintaining synchronism of the power winding are handled by the control winding, which also provides the wind-power distribution between the winding sets.

The proposed concept has two main drawbacks arising from its direct grid connection. One is that the reactive power generation of the power winding cannot be controlled during operation, owing to the absence of the field winding and power converter. This drawback can be overcome by considering the reactive power during the design of the generator

(the detailed study is provided in Section III). Moreover, the DC/AC converter can supply the reactive power demand to the extent its capacity allows. Another drawback is its lack of maximum power-point tracking, as directly grid-connected synchronous machines must rotate at a constant speed, regardless of the wind speed. Therefore, power coefficient of the wind-turbine blades will not be optimum for all wind speed values. However, it is known that wind turbines with MPPT feature cannot follow the maximum power point beyond the rated speed where the rated output power is fixed by the generator. Therefore, the MPPT feature alone is not a good indicator for making a fair comparison between fixed and variable speed wind turbines. Instead, long term capacity factor should be analyzed, which depends also on the turbine diameter, generator rated power and the probability density function of the wind speed at the site. On the other hand, the proposed DFPMSG does not need a gear box. Moreover, the power winding can be connected to the grid directly without needing a power converter, which significantly reduces losses. These two improvements increase the power efficiency especially beyond the rated speed, and in turn, may increase the capacity factor significantly for optimum designed systems. In the proposed DFPMSG system, the optimum number of poles can be selected according to the wind regime of the site, which also improves the capacity factor.

A. KEY FEATURES OF THE PROPOSED SYSTEM

In addition to the common advantages of PMSG, the proposed system has the unique features stated below.

- The cost of the power converter is about 7%-12% of the total cost of the wind-turbine system at the MW power level [11]. The reduction in initial cost and increase in system efficiency can be achieved due to the decreased rated power of the converter.
- Although the power winding set is uncontrollable, the power winding set can be manipulated indirectly by interfering with the torque produced by the control winding. Thus, the power produced by the winding sets can be arranged by transferring wind power to the grid as efficiently as possible. Furthermore, the life of the power converters can be extended, and the winding temperatures can be maintained within safe limits via thermal-management algorithms.
- Both the winding configuration and double-fed structure improve the fault tolerance of the DFPMSG.
- Fixed-speed systems are less complex in terms of turbine design and system control.
- Directly grid-connected generators without power converters have difficulties synchronizing with the grid and overcoming sudden wind-speed changes. Both grid synchronization and oscillation damping in DFPMSGs can controlled with the aid of a controllable winding set.

B. ANALYTICAL MODEL OF THE MACHINE

Decoupling between winding sets for double-fed electrical machines can be ensured by single layer concentrated winding topology [31]. Thus, winding sets of the DFPMSG can be considered as two independent machines in terms of electrical equations. Voltage and torque equations of PM machines in [32] can be used separately for the power and control windings.

$$\begin{bmatrix} V_{qs} \\ V_{ds} \end{bmatrix} = \begin{bmatrix} R_s + pL_q & wL_d \\ -wL_q & R_s + pL_d \end{bmatrix} \begin{bmatrix} i_q \\ i_d \end{bmatrix} + \begin{bmatrix} w\lambda_m \\ 0 \end{bmatrix} \quad (1)$$

$$T_e = \frac{3}{2}\frac{P}{2}\left[\lambda_m i_q + \left(L_d - L_q\right) i_d i_q\right] \quad (2)$$

The angle used for the transformation of circuit variables to the d-q reference frame is not the same for winding sets, but has a fixed difference. The angle difference between winding sets is given by (3).

$$\theta_d = \frac{4\pi \times n_c}{Q \times t_s}, \quad (3)$$

where n_c is the number of coils per phase, Q is the slot number and t_s is the symmetry multiplier of the stator.

Although the winding sets of DFPMSG are electrically and magnetically decoupled, the generated torques drive the same rotor. Thus, the torque and speed may be related as

$$T_{e,power} + T_{e,control} + T_{wind} = J\frac{dw}{dt} + Bw, \quad (4)$$

where $T_{e,power}$ is the torque generated by the power winding, $T_{e,control}$ is the torque generated by the control winding, T_{wind} is the wind torque, J is the inertia of the rotor and B is friction coefficient.

C. CONVERTER SYSTEM

The bidirectional converters used in the system are two-level voltage-source inverters with six active switches. The grid- and generator-side converters that control the power flow by field-orientation control and space-vector modulation are shown in Fig. 2. The d–q axis currents are regulated by PI controller, whose coefficients are calculated with the Ziegler–Nichols method [33].

The generator-side converter handles managing the wind power by generating the desired torque commanded by the control algorithm detailed in Section IV. Furthermore, I_d is controlled to obtain maximum torque per ampere.

The grid-side converter manages bidirectional power flow while the control winding acts as a motor or generator. Power flow control is realized by maintaining the voltage of the DC bus at an adequate constant level. The power demand of the generator side is provided by keeping the DC bus voltage level steady. Further, the reactive power demand to maintain a high power factor for the whole system can be provided by the grid-side converter.

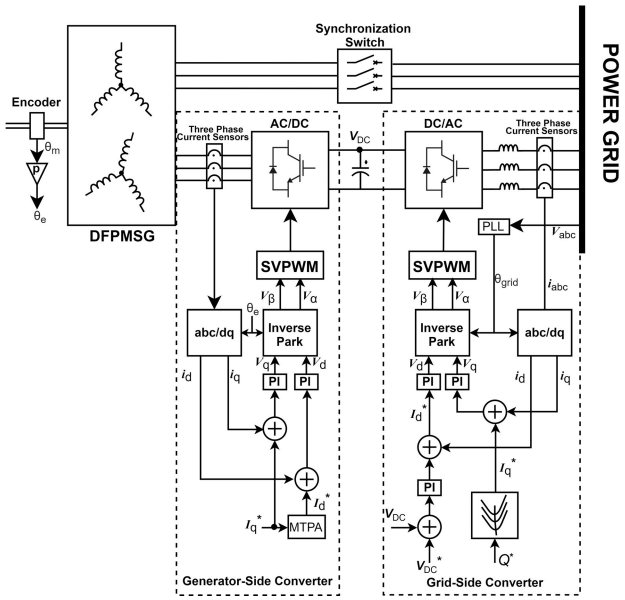

FIGURE 2. Control diagram of the converters.

TABLE 1. Comparison of wind turbine generator concepts 1:Poor, 2:Fair, 3:Good, 4:Excellent.

Parameters		DFIG	BDFM	PMSG	DFPMSG
Torque density		2	1	3	3
Power factor		2	3	4	4
Power quality		3	1	2	3
Reliability		2	3	4	4
Stability		3	3	3	3
Cost	Generator	3	2	1	1
	Converter	3	3	1	2
	Gearbox	1	1	4	4
	Maintanence	1	2	3	3
Grid faults	FRT	2	2	4	3
	Faults current	3	3	2	3
Energy yield	Speed range	2	2	4	1
	Drive train eff.	3	3	4	4

D. COMPARISON OF DFPMSG WITH OTHER GENERATOR SYSTEMS

The proposed concept is compared against direct-drive PMSG and double-fed concepts for WECS in terms of cost and operation. Comparison criteria and ratings are summarized in Table 1.

- PM machines are more advantageous than conventional induction machines (IM) in terms of torque density. However, the torque density numbers are relatively lower in BDFMs compared with the counterparts [34].
- Reactive power demand is met by power converters in the systems with PMSG. DFPMSG is designed to have a high power factor. Although the DFPMSG system has reduced size converter, control winding can provide relatively low reactive power demand.
- Since BDFMs are designed to interact two main harmonic components, they have poor power quality. This eventually causes additional torque ripple and unbalanced magnetic pull [35], [36].
- Considering the number of components, brushes, gearbox and mechanical vibrations etc., DFIG is less reliable than others [37].
- Directly grid-connected systems are weak in terms of stability against sudden wind changes. Although the proposed system has a direct grid connection, control winding helps to assure stability.
- Direct drive systems have to produce higher torque than geared systems to meet same electrical power. Therefore, dimensions of the direct-drive generators should be larger than geared systems. This makes direct-drive systems to be disadvantageous in terms of generator costs. Nevertheless, the gearbox and its maintenance costs are eliminated. On the other hand, systems with brushes have higher maintenance costs. Another factor that determines the cost is the converter size. In this respect, full scale systems are more disadvantageous.
- WECS with a full converter has full control over the currents. Therefore, they can stay connected to the grid when a short-circuit faults occur. On the other hand, they cannot provide faults currents above the rated current [38]. Having a partial-scale power converter in the proposed system makes it disadvantageous with regard to fault ride through (FRT), but advantageous as far as the fault current magnitude is concerned. The disadvantages of the proposed system for FRT can be compensated with concentrated winding topology which yields high self-inductance and low mutual inductance in the generator [39].
- The DFPMSG is constant-speed WECS while DFIG and BDFM are semi-variable speed and PMSG is full-variable speed. The wide speed range, which allows MPPT to be performed at low wind speeds, increases energy harvesting. It should be emphasized that the width of the speed range is not limitless and dictated by the MPPT voltage range of the converter. In [40], drive train efficiency comparison is made between BDFM, DFIG and PMSG taking the efficiencies of gearbox, converter and generator into account. Drive train efficiency of the proposed system is similar to direct-drive PMSG besides converter loss is lower than the PMSG.

In [21], it is shown that direct-drive systems have a higher energy yield than geared systems. In [41], it is stated that direct-drive systems are more advantageous in terms of cost of energy which includes transportation, installation, and maintenance cost, etc. for offshore wind turbines. Since the proposed system is direct drive, it is anticipated to be superior with regard to the cost of energy.

III. DESIGN REQUIREMENTS OF THE DFPMSG

In WECS, the rated power and speed of the generators cannot be determined solely by electrical dynamics without a mechanical aspect. Especially in directly grid-connected PMSGs, pole numbers determines the operation speed that directly affects the aerodynamic behavior of wind turbine. Thus, the parameters such as the characteristic of the turbine

and wind regime of the site must be taken into account when determining the number of poles, in other words, rated speed. In this section, first, the slot/pole combination determination is described for directly grid-coupled PMSGs. The correlation between the rated power and pole number selection is also discussed.

A. RATED POWER AND RATED SPEED

Power captured from wind is related to the aerodynamic model of the wind turbine. The mechanical power generated by the wind is given by (5).

$$P_m = \frac{1}{2}\rho A v^3 C_p(\lambda, \beta), \tag{5}$$

where P_m is mechanical power, ρ is air density, A is the swept area of turbine blades, v is wind speed and C_p denotes the power coefficient of the wind-turbine blades. C_p can be represented as the function given by (6) which describes the nonlinear relationship between the blade pitch angle (β) and tip speed ratio (λ) [42]. The coefficients of C_p for different applications are given in [43].

$$C_p(\lambda, \beta) = c_1\left(\frac{c_2}{\lambda_i} - c_3\beta - c_4\beta^{c_5} - c_6\right) * \exp\left(\frac{-c_7}{\lambda_i}\right) \tag{6}$$

$$\lambda_i = \left[\frac{1}{(\lambda + c_8\beta)} - \frac{c_9}{\left(\beta^3 + 1\right)}\right]^{-1} \tag{7}$$

Tip speed ratio can be expressed as

$$\lambda = \frac{R * \omega_m}{v}, \tag{8}$$

where ω_m is the mechanical speed of the rotor and R is the radius of the blades. The relationship between the electrical and mechanical speeds is given by

$$\omega_m = \frac{2}{p}\omega_e, \tag{9}$$

where p is the number of poles. As demonstrated by (9), the rotor's mechanical speed is dependent on pole number. Given that the electrical frequency is nearly constant in directly grid-connected applications, the number of poles in the generators determines the operation speed. Therefore, the mechanical power P_m should be a function of pole number, as well.

The mean mechanical power is computed using the probability distribution of wind speed, as follows:

$$P_{mean} = \int_{v_{ci}}^{v_{co}} P_m(v)F(v)dv, \tag{10}$$

where v_{ci} and v_{co} are is cut-in and the cut-out wind speed of the wind turbine, respectively, and $F(v)$ is the probability density function of the wind speed at the site.

The torque generated by the wind to keep the turbine blades turning is not sufficient at low wind speeds. The minimum wind speed, where the mechanical power begins to take a positive value (cut-in speed), can be derived by finding the roots of (5). The cut-out speed depends on whether the machine is operating in the reliable wind-speed region, where the pitch control of blades is stable. In addition, the thermal limit of the machine and power angle stability limit of the generators are other important factors determining the cut-out range of the system.

TABLE 2. Calculation parameters.

Parameters	Value
Radius of the Blades(m)	3
Pitch Angle β	0°
Air Density (kg/m3)	1.225
Scale Parameter	4.657
Shape Parameter	1.4803
Cut-out Wind Speed (m/s)	20

Weibull distribution is widely used to fit the real wind-speed data for estimation and analysis. Weibull distribution is a two-parameter function, and is given by (11).

$$F(v) = \left(\frac{k}{c}\right)\left(\frac{v}{c}\right)^{k-1}\exp\left[-\left(\frac{v}{c}\right)^k\right], \tag{11}$$

where v is the wind speed, k is the shape parameter and c is the scale parameter. The parameters of the Weibull function can be calculated using different methods that are detailed in [44].

Another design decision of WECS is the capacity factor, which is simply the mean power generated, divided by the rated peak power of the generator. Typical capacity factor values are between 20% and 40% [45]. Because the capacity factor affects the initial cost and payback period, its determination is an economical optimization problem and is not within the scope of this study. For both a fixed capacity factor and fixed rated power, the annual mean power is calculated for each possible number of poles using the Weibull function, which is constructed with the wind data collected from a site in Soke, Turkey, every 10 min for a year [46]. The shape and scale parameters are calculated as 1.4803 and 4.657, respectively, using the empirical method of Justus [47] according to Soke wind data. Fig. 3 shows the annual mean mechanical powers for different numbers of poles for a fixed capacity factor of 0.3 and Fig. 4 shows the annual mean mechanical powers for a fixed rated power of 5 kW. The parameters using in the calculations are listed in Table 2. According to calculations, the system with 4.8-kW rated power and 46 poles has the highest annual mean power. In the case of 5-kW rated power, the annual mean power is increased to 1468 W, whereas, the capacity factor remains nearly the same. Also, the optimum number of poles does not change.

The trade-off between the initial cost and annual mean power requires an economical optimization study. The capacity factor of 0.2936 is within reasonable values; thus, the rated power is selected as 5 kW and the rated speed is determined per 46 poles.

B. MAGNETIC DECOUPLING BETWEEN WINDING SETS

The pole number cannot be determined without considering the winding factor of the generator. This enforces a

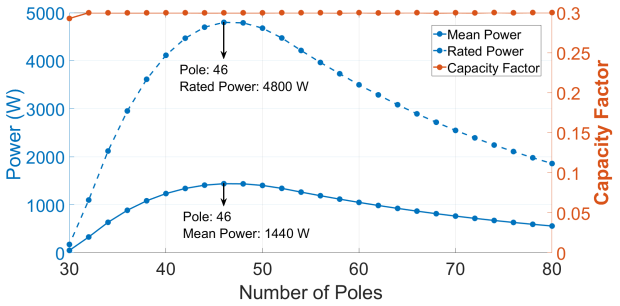

FIGURE 3. Mean power versus pole numbers for fixed capacity factor.

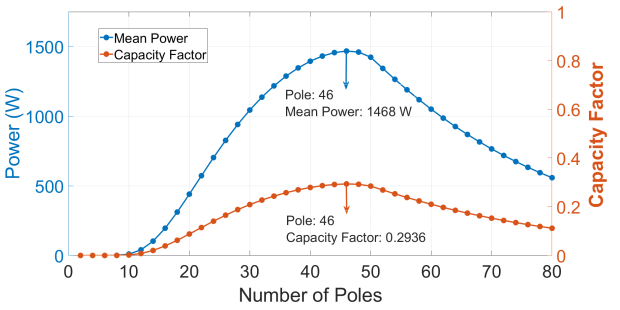

FIGURE 4. Mean power versus pole numbers for 5-kW rated power.

decision regarding the slot and pole number combination, rather than the pole number alone. The preferred winding configuration of the generator is nonoverlapping concentrated windings with tooth-wound coils to ensure decoupling between the winding sets, as well as for other advantages, such as high-power density and high efficiency [39]. The detailed calculation of the winding factor for fractional-slot concentrated windings can be found in [48]. The slot/pole combination of 48/46, which has a high winding factor, is an appropriate choice, and also has a low unbalanced magnetic force according to [49].

Specific to the proposed system, it is important that there is no mutual inductance between the winding sets in order to realize the dual port structure and control the power of the winding sets. Reduction of the mutual inductance between phases for fractional slot winding configurations of synchronous machines is described in [50]. The ratio of $Q/(2t)$ has to be even for minimum mutual inductance in single layer configurations. Where t is the greatest common divisor of slot number and pole pairs. The slot/pole combination of 48/46 fulfills this requirement.

The mutual inductance between any two phases can be calculated as follows [51]:

$$M_{ab} = \frac{\mu_0 r_g l}{g} \int_0^{2\pi} N_a(\theta) N_b(\theta) d\theta \tag{12}$$

where μ_0 is the permeability of air, r_g is the airgap radius, l is the machine active length, g is the air gap length, $N_a(\theta)$ and $N_b(\theta)$ are the winding functions of phases a and b.

The winding function of phase A of both winding sets is shown in Fig. 5. In theory, there is no mutual inductance between the winding sets, since the product of the winding functions yields zero when (12) is evaluated to find mutual coupling between control and power windings as devised in the proposed system.

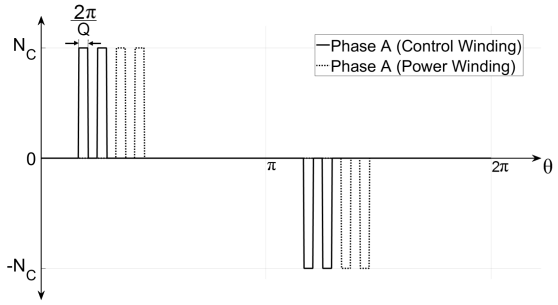

FIGURE 5. Winding functions of the same phase of winding sets.

C. BACK EMF AND SYNCHRONOUS INDUCTANCE

For machines directly connected to the grid, the back EMF value is a critical parameter for synchronization and power transmission. Similarly, the synchronous inductance value affects the power transmission, stability limit, and reactive power of the machine. These values should be adjusted to the desired values based on parameters such as the number of turns, machine dimensions, and magnet dimensions.

The active and reactive power equations are given by (13) and (14), respectively [52].

$$P = \frac{3V_T E_A}{X_S} \sin(\delta), \tag{13}$$

$$Q = \frac{3V_T}{X_S} \left(E_A \cos(\delta) - V_T\right), \tag{14}$$

where V_T is terminal voltage, E_A is induced back EMF, δ is the power angle of the generator and X_S is synchronous reactance.

The analogy between DC machines and PM machines is explained in [32]. In DC machines, the induced back EMF is

$$E_A = k_m \phi \, \omega_m, \tag{15}$$

where k_m is the machine constant and ϕ is magnetic flux. Because ω_m is nearly constant and ϕ can be considered constant, due to the direct grid connection and the PMs, respectively, E_A can be assumed constant during operation. In addition, the grid frequency and voltage are assumed to be constant. Thus, X_S and V_T are taken as constant during the calculations. For the design stage of the generator, E_A and X_S are dependent on factors including the number of turns, diameter and length of the machine, and magnet thickness, which are all known after designing the machine. Because of this, the relation between the active power and power angle are known after the design is completed. The power angle of a generator that generates 2.5 kW is sketched for different E_A

and L_S values in Fig. 6 using (13). The reactive power can be calculated from (14) by using these power-angle values. The reactive power of the same generator is given in Fig. 7 for different E_A and L_S values. The generated power P, terminal voltage V_T, and electrical frequency are taken as 2500 W, 220 V_{rms}, and 50 Hz in calculations, respectively. Half of the rated power is used in the calculations because each winding set is sized for half of the rated power.

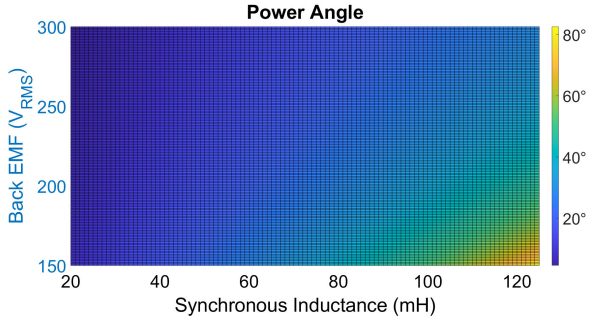

FIGURE 6. Power angles for different back EMF and synchronous inductance.

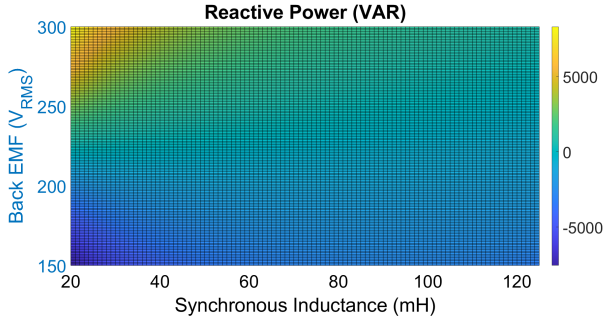

FIGURE 7. Reactive powers for different back EMF and synchronous inductance.

In the design stage, the values of E_A and L_S could be arranged so that reactive power is not produced when the machine generates the rated active power. The value of E_A that sets the reactive power to zero is given by (16).

$$E_A^\star = \frac{V_T}{\cos(\delta)} \tag{16}$$

Then, (13) is rearranged to isolate the power angle.

$$\delta = \arcsin\left(\frac{PX_S}{3V_T E_A}\right) \tag{17}$$

$E_A^\star$ can be expressed as follows after trigonometric operations:

$$E_A^\star = \frac{\sqrt{9V_T^4 + P^2X_S^2}}{3V_T}. \tag{18}$$

The back EMF calculated from (18) is sketched in Fig 8. The power factor is unity at the rated power for the machines with the back EMF and L_S values illustrated in Fig. 8. Furthermore, a smooth synchronization process can be confirmed because the back EMF values along the line are close to V_T.

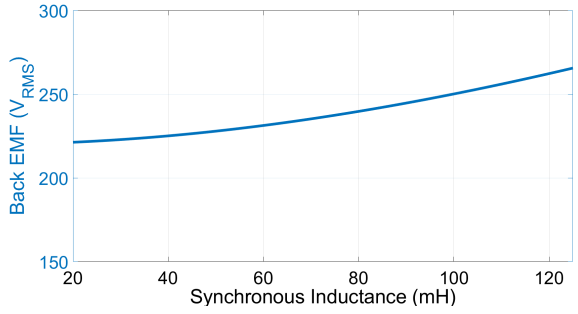

FIGURE 8. Zero-reactive-power curve.

The back EMF and synchronous inductance values should be selected near the values of the zero-reactive-power curve to maintain a high power factor. Furthermore, the power angle must be considered in the design process. A low power angle yields an inefficient design, whereas a high power angle risks exceeding the stability limit after a torque disturbance. The machine parameters, such as the length, rotor diameter, and number of turns, are arranged to achieve desired back EMF and L_S values according to the analytical findings.

D. OTHER PARAMETERS

In the previous section, the machine output power is calculated according to the wind distribution data. The basic parameters of the machine, such as its rated speed, torque, rotor outer diameter, and the core length, are determined depending on the output power. Both winding sets comprise an equal number of identical coils and provide equal output power. The required nominal torque value under a constant mechanical speed for a specified output power can be calculated by (19).

$$T = \frac{P}{\omega} = \frac{5000}{13.66} = 366.056Nm \tag{19}$$

The stator structure of the proposed double-fed generator is formed from modular E-cores, and the rotor structure consists of modular surface-mounted PM poles. The conceptual design and parameters of the modular machine are shown in Fig. 9.

After the rotor diameter is calculated using the basic torque equation, the pole width can be calculated by (20) depending on the rotor outer diameter, number of poles, and magnet height (h_m).

$$\omega_p = (D_r - h_m \times 1.9816) \times sin(\frac{180}{2 \times p}) \tag{20}$$

The magnet width (w_m) and the distance between magnets (w_e) can be determined using equations (21) and (22) with respect to the embrace ratio (e), respectively.

$$\omega_m = \omega_p \times e \tag{21}$$

$$\omega_e = \omega_p \times (1 - e) \tag{22}$$

Because the stator and rotor geometries are polygons, the stator inner diameter (D_{si}) should be calculated by taking

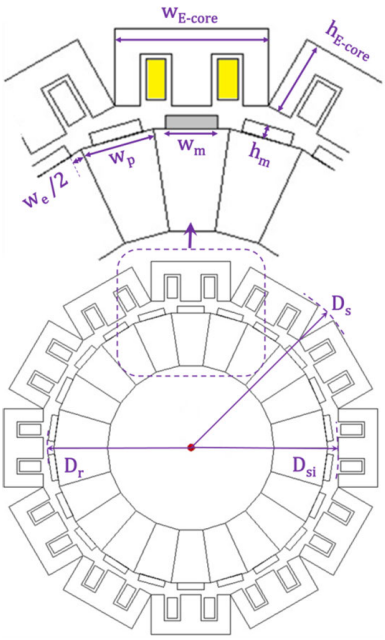

FIGURE 9. Basic concept of the modular PM machine.

the lowest airgap value. The E-core width (ω_{E-core}) can be calculated using (23) depending on the stator's inner diameter and the number of E-cores (N_{E-core}). The outer diameter of the stator (D_s) can be approximated using (24) depending on the E-core height (h_{E-core}).

$$\omega_{E-core} = D_{si} \times tan(\frac{180}{N_{E-core}}) \tag{23}$$

$$D_{si} = \frac{\omega_{E-core}}{sin(\frac{180}{N_{E-core}})} + h_{E-core} \times 1.9816 \tag{24}$$

In [53], the authors perform a detailed study on the determination and optimization of the E-core dimensions in terms of modularity and scalability. The generator parameters determined within the design study are given in Table 3.

E. FINITE-ELEMENT MODEL AND ANALYSIS

The proposed DFPMSG has been modeled in ANSYS/Maxwell software, and electromagnetic analyses have been performed. The DFPMSG model and the coil placement of the winding sets are shown in Fig. 10.

The E-cores that form the stator are designed in the simplest form possible to maximize the ease of manufacturing and assembly. Therefore, the teeth and slots of the E-core have a rectangular shape. The modular structure causes more severe airgap permeance variation than that of conventional surface-mounted PM machines. As shown in Fig. 9, in addition to the slot effect, a varying airgap length is inevitable with the proposed E-core. The cogging torque and torque ripple have been optimized with the magnet width and magnet skew angle. The magnet length is divided into three parts and skewing is performed in three steps. Figure 11 shows the average torque and torque ripple percentage variations for the skew angle. At 0.4° of skew angle, the average torque value

TABLE 3. Machine design parameters.

Parameter	Value	Parameter	Value
E-Core Width (mm)	54.83	Output power (W)	5000
E-Core Height (mm)	39.54	Rated torque (Nm)	366
E-Core Length (mm)	150	Rated speed (rpm)	130.43
Air-gap Length (mm)	1.56	Electrical frequency (Hz)	50
Rotor Outer Diameter (mm)	374	Number of turns	110
Rotor Core Length (mm)	150	Wire diameter (mm)	1.15
Magnet Width (mm)	21.9	Rs-phase resistance (Ω)	3.32
Magnet Height (mm)	5	Synchronous-inductance (mH)	62
Rotor Skew Angle (°)	0.4	Back EMF (V_{rms})	226.72
Slot / Pole Combination	48 / 46	B_r of magnet (T)	1.23
Net Slot Area (mm^2)	293.73	Tooth flux density (T)	1.5
Slot Fill Factor (%)	53.18		

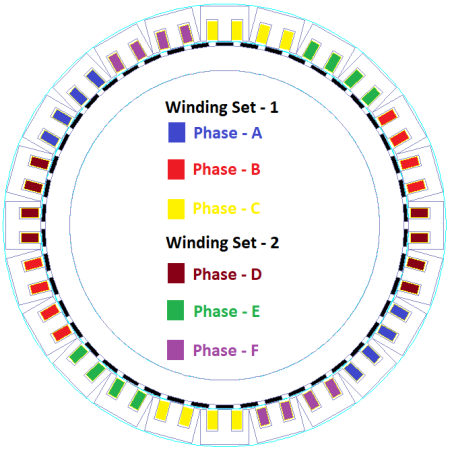

FIGURE 10. Two-dimensional model of DFPMSG and coil arrangement.

reaches the desired value and the torque ripple percentage is minimized.

The torque ripple percentage and average torque variations depending on the magnet width are shown in Fig. 12 for a constant magnet height constant. Considering the required average torque value, the lowest torque ripple percentage is obtained for a 21.9-mm magnet width.

The analysis results are obtained when one of the winding sets is fully loaded. The induced back EMF and torque waveforms are given in Figs. 13 and 14, respectively. As seen from Fig. 13, the peak value of the induced back EMF is 320 V. The average torque is approximately 185 Nm, and the torque ripple is approximately 3.5%.

In Fig. 15, the magnetic flux-density distribution of the designed machine under full load is depicted. The flux density in the yoke of the rotor and E-cores is 400-500 mT, and is approximately 1500 mT in the E-core teeth. According to the flux-density distribution, magnetic saturation does not occur in any region of the machine.

IV. SYSTEM-CONTROL ALGORITHM

A. START-UP AND GRID SYNCHRONIZATION

The proposed wind-powered generator system requires a start-up sequence to connect the DFPMSG to the grid. For this

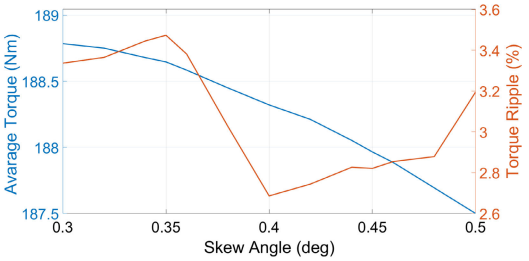

FIGURE 11. Effects of skew angle on output torque.

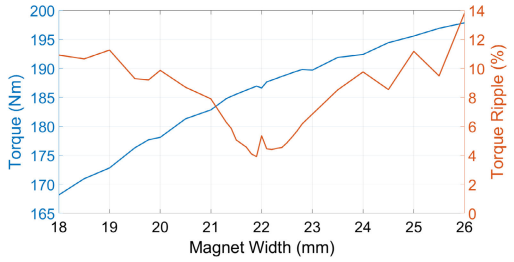

FIGURE 12. Effects of magnet width on output torque.

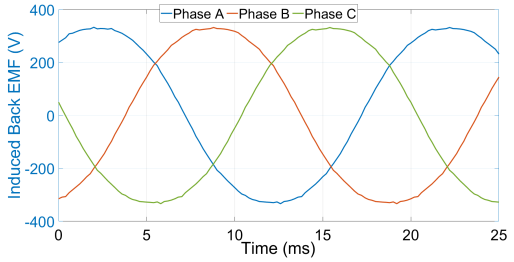

FIGURE 13. Induced back EMF at rated speed.

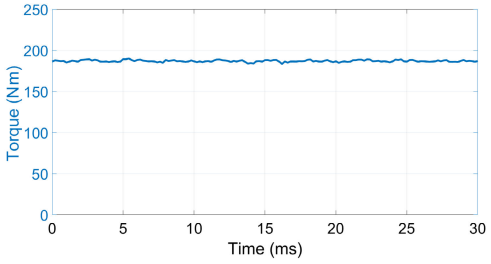

FIGURE 14. Torque of a winding set at full load.

purpose, a back-to-back converter drives the DFPMSG as a motor through the control winding, using grid power. The control algorithm speeds up the DFPMSG from zero to synchronous speed progressively and equates the frequency of generated voltage to the grid frequency. Once phase synchronization is achieved, the synchronization switch connects the power winding to the grid without dangerous inrush current. It should be noted that if the shaft (wind) power of the DFPMSG is higher than the back-to-back converter's rated power, the speed cannot be regulated by the converter. In this case, synchronization cannot be achieved, and

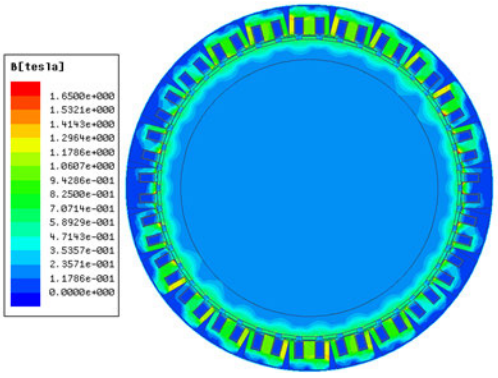

FIGURE 15. Magnetic flux-density distribution of DFPMSG.

more importantly, the speed may increase progressively and reach a dangerous level for the converter. For this reason, the pitch angle of the blades should be increased during the start-up sequence to ensure that the shaft power remains safely below the converter's rated power. Once synchronization is achieved, the rated power of power winding is added to the control winding, and then the total power capacity of the generator is considerably increased. Therefore, after the start-up sequence, the pitch angle can be returned to its original position.

B. TORQUE MANAGEMENT ALGORITHM

The DFPMSG operates at a constant shaft speed. However, if the wind speed reaches the rated value, the shaft torque must be limited to below the generator's rated torque by controlling the pitch angle of the blades. In this paper, it is assumed that the pitch-control system works well; thus, the turbine mechanical power input is always under the generator rated power. While the machine is synchronized with the grid and the input torque is below the rated power, grid frequency dictates the mechanical speed. DFPMSG responds to torque changes by increasing or decreasing the power angle. Consequently, the speed-control system is not essential for the proposed DFPMSG generator. At steady state, the torque equation (25) becomes the following by ignoring friction losses:

$$T_{e,power} + T_{e,control} + T_{wind} = 0. \tag{25}$$

If the winding currents are measured, electrical torques can be calculated using (2). Thus, the wind torque can be obtained from (25). It can be concluded from (25) that the wind power is shared between the control and power windings. However, the power efficiencies for these power paths are not equal. As can be seen from the measured efficiencies shown in Fig. 16, the control winding's power efficiency is lower than that of the power winding, mainly due to back-to-back converter losses.

In the steady-state operation, if the produced torque of the control winding is changed slightly, the power winding takes on the rest of the wind torque. Three different wind torque

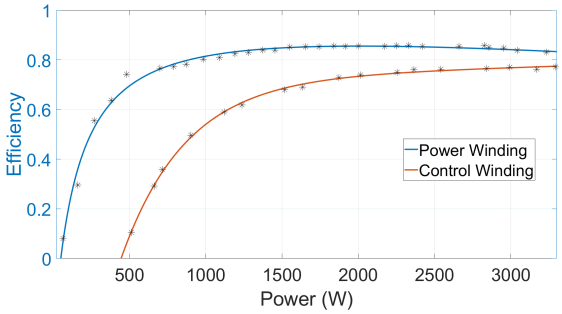

FIGURE 16. Fitted efficiency curves and experimental efficiency data of the winding sets.

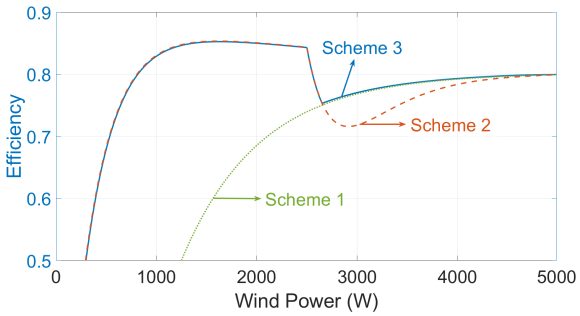

FIGURE 17. Efficiencies of the schemes.

sharing schemes between winding sets, without exceeding the rated powers, are investigated.

- Scheme 1: The winding sets share the input wind power equally.
- Scheme 2: Only the power winding generates energy between 0 and 2500 W of input wind power. Above 2500 W of wind power, the power winding takes 2500 W, and control winding takes the remaining input wind power.
- Scheme 3: The wind power is distributed to maximize the overall efficiency.

The following equation is maximized to realize Scheme 3:

$$\eta_s = \frac{P_c \eta_{cc} + P_p \eta_p}{P_w}, \tag{26}$$

where P_c, P_p, and P_w are the control winding, power winding, and input wind power, respectively; η_{cc} is the control winding efficiency with the converter; and η_p is the power winding efficiency.

The optimum system efficiency is found by an offline brute-force search method according to experimental efficiencies. The calculated system efficiencies for all schemes are shown in Fig. 17. Scheme 3 provides higher system efficiency than Schemes 1 and 2.

The block diagram of torque distribution to realize the schemes is designed as shown in Fig. 18. The algorithm first calculates electrical torques $T_{e,power}$ and $T_{e,control}$ using the direct and quadrature components of the measured winding currents using (2) and then computes the wind torque using (25). Afterward, the reference torque for the control winding, $T^{\star}_{control}$, is calculated according to schemes using the computed wind power. $T^{\star}_{control}$ is converted to the I_q quadrature current by multiplication with K (calculated using (2)). The rate limiter prevents sharp dynamic power disturbances and provides a soft power transition.

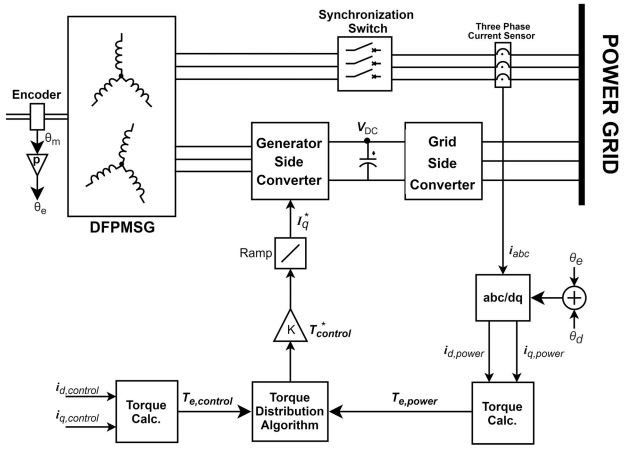

FIGURE 18. Block diagram of the control algorithm.

V. EXPERIMENTAL RESULTS

The prototype of the DFPMSG, whose parameters are given in Table 3, is manufactured. The experimental setup to verify the proposed concept, DFPMSG, and power converters is depicted in Fig. 19. A four-pole, 11-kW rated power, induction motor (IM) and a gearbox with gear ratio of 1:11 is used to emulate a wind turbine. A four-quadrant motor driver (Schneider ATV930D11N4 with regenerative unit) is used to control of the IM. The input torque is measured by HBM T22 torque sensor mounted between the induction motor and DFPMSG. Measuring range of torque sensor is 1000-Nm with 0.5% sensitivity. The rotor speed and position are measured by an 8192 pulse per revolution incremental encoder. The output powers are measured by power-quality analyzer and network analyzer. Back-to-back (AC/DC-to-DC/AC) converter with 2.5-kW rated power is used to bidirectional energy flow of control winding.

A three-phase balanced current is applied to a winding set, and the phase-phase voltage of the other winding set is measured while rotor is locked, to determine the mutual inductance. A screenshot of the scope is shown in Fig. 20. It is measured that while 30.9% of the nominal current flows through one winding set, 2.1% of the nominal back EMF value is induced on the other winding set. The reason of existence of the mutual inductance, which should theoretically be close to zero in classical one-piece stator structure, is that the stator consists of E-cores which slightly increases the leakage fluxes and mutual inductance.

Control performance of the converter control algorithm (given in Fig. 2) are verified with experimental study. In Fig. 21, a step function is applied to generator side

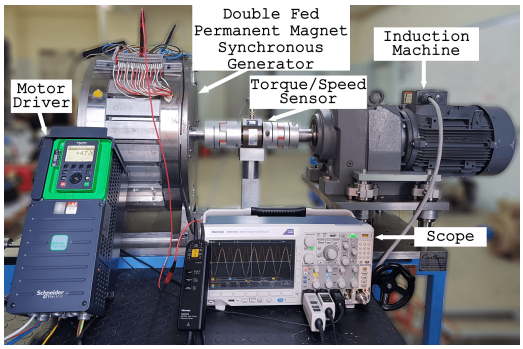

(a)

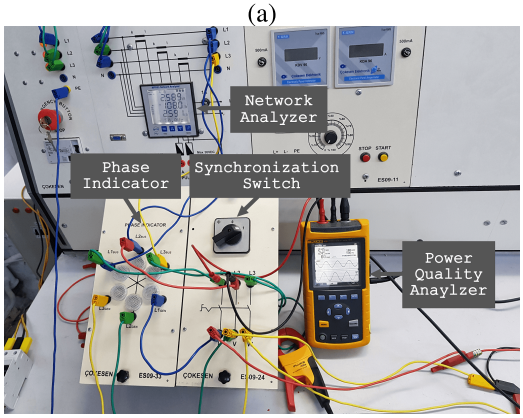

(b)

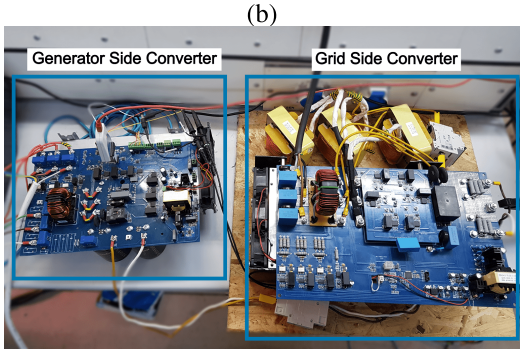

(c)

FIGURE 19. Experimental setup. a) part 1, b) part 2, c) part 3.

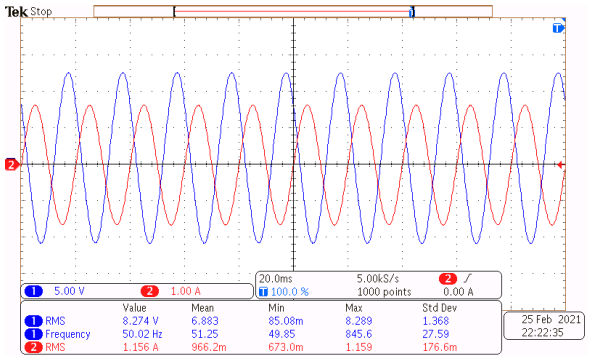

FIGURE 20. Mutual inductance test.

converter's I_d and I_q reference while grid side converter is keeping V_{DC} bus about 700-V. Reference of I_d is switched from 0.5-A to 2-A while reference of I_q is constant. I_d current

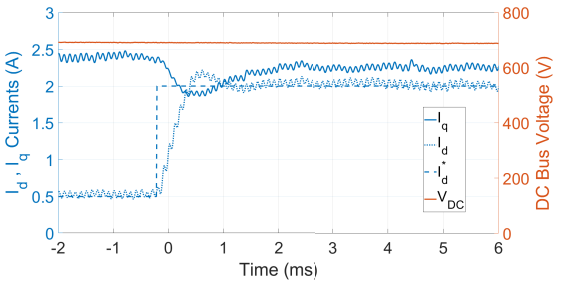

(a)

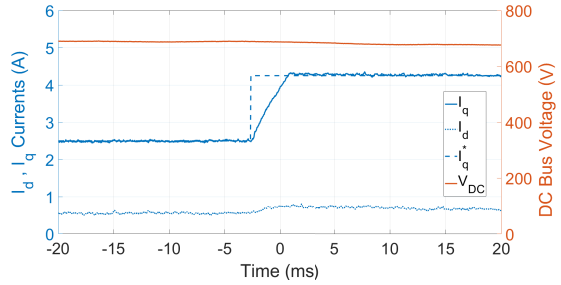

(b)

FIGURE 21. Dynamic response of the power converters a) to the step-input of I_d^* b) to the step-input of I_q^*.

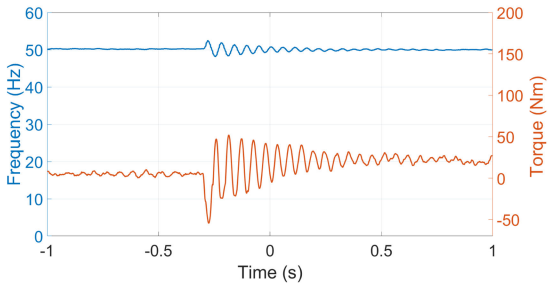

FIGURE 22. Torque and frequency oscillations while the synchronism is starting.

settling time is measured as 2.2-ms (see Fig. 21 (a)). Reference of I_q is switched from 2.5-A to 4.25-A while reference of I_d is constant. I_q current settling time is measured as 4.1-ms (see Fig. 21 (b)). Keeping DC bus voltage steady is successfully managed by grid side converter in both cases. The experimental results confirm that the control method and the selected PI coefficients are suitable.

Mechanical torque and electrical frequency variations in the synchronization process are shown in Fig. 22. Synchronization is accomplished with an overshoot of 5% and a settling time of 500-ms for electrical frequency.

A step torque input is applied to the system for analyzing the dynamic behaviour of the system. The measured mechanical torque and electrical frequency variations are shown in Fig. 23. The system manages to transfer the input torque with the oscillation below 0.3-Hz in electrical frequency. The fact of the matter is that step wind speed change is not natural. Therefore, it is anticipated that the system will be less affected under extreme wind speed changes like gusts.

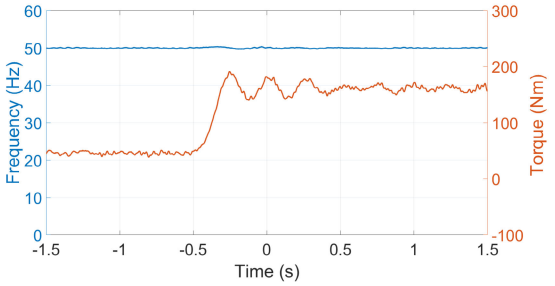

FIGURE 23. Dynamic behavior of the system for step input of mechanical torque.

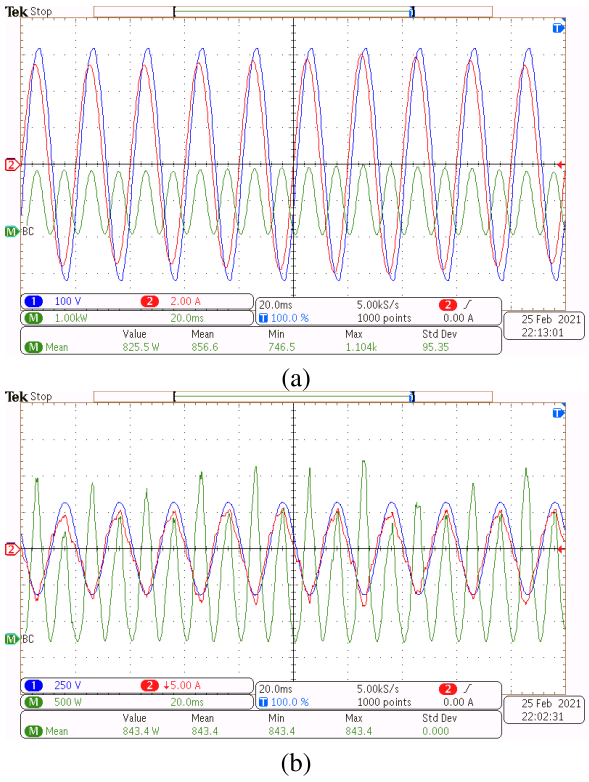

FIGURE 24. Phase A output power of a) power winding set b) control winding through converter.

Both power winding and control winding through converter are tested separately at rated power. The voltages, currents, and instantaneous output powers are indicated in Fig. 24. The power factor of the power winding is 0.94, owing to the consideration of reactive power in the design stage (see Fig. 24 (a)). Figure 24 (b) shows that the grid-side converter works well and produces almost zero reactive power.

Schemes 1, 2 and 3, as mentioned in Section IV, are implemented in the system-control algorithm. The torque distribution between winding sets is shown in Figs. 25, 26 and 27 for Schemes 1, 2 and 3, respectively, under varying input torques.

Input torque varies with ramps between 0 and 330 Nm in the experiment of Scheme 1 as shown in Fig. 25. Control winding successfully manages the equal distribution of the

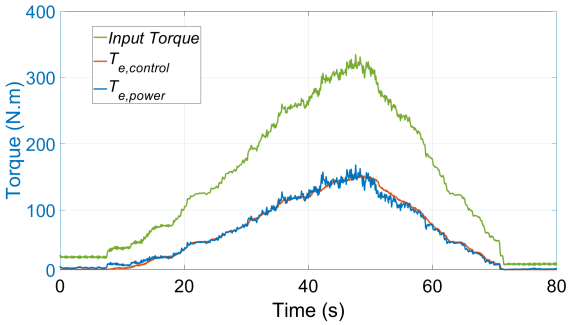

FIGURE 25. Torque-distribution scheme 1.

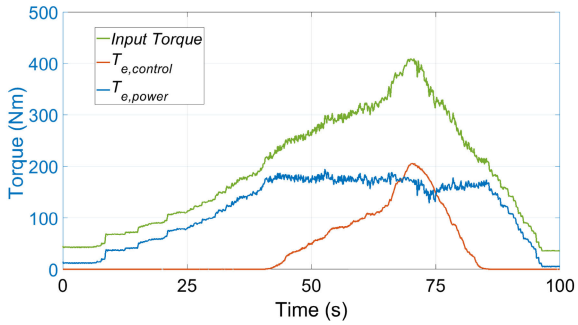

FIGURE 26. Torque-distribution scheme 2.

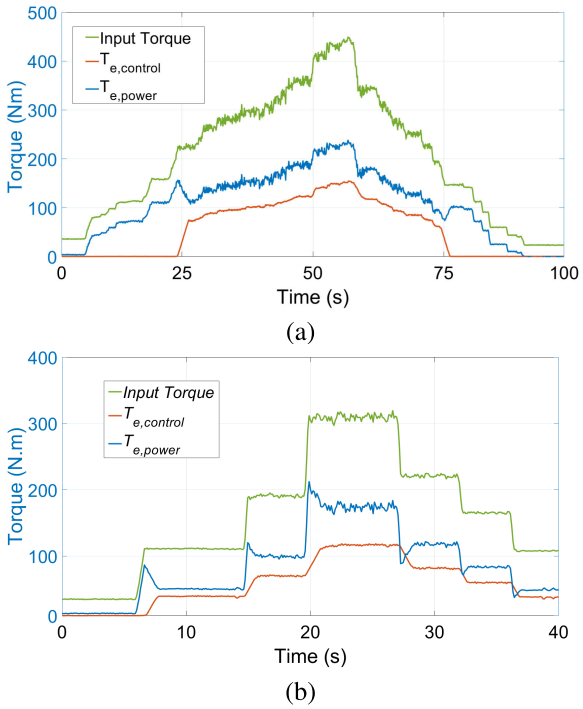

FIGURE 27. Torque-distribution scheme 3 (a) Experiment 1 (b) Experiment 2.

input torque between the winding sets. Experimental result of Scheme 2 is shown in Fig. 26. The control winding does not involve power sharing until the power winding reaches

its nominal torque value of 183.12 Nm. The control winding begins to take the remaining input power after 42 s. Thus, the torque of the power winding is kept constant between 42 and 85 s. In the experimental implementation of Scheme 3, two different torque profiles have been applied while the input torque is ramp-like in the first experiment, it consists of step variations in second experiment.

The control winding involves power sharing at 24 s for experiment 1. After that, the control winding arranges the torque distribution according to the optimum efficiency curve. When step variation is occurred at input torque, power winding response immediately for experiment 2. Then control winding takes the specific torque values according to scheme 3 with a ramp of 30 Nm per second. The slope of the ramp can be adjusted as steeper or more gradual according to desired response. There are small ripples on the power winding torque during torque sharing. The mutual inductance between winding sets causes torque ripple, which does not appear on the control winding side. This demonstrates the robustness of the current regulators in the generator-side converter. In summary, the results show that the input torque can be shared freely between the winding sets within the limits.

VI. CONCLUSION

In this study, a dual-port WECS is proposed. The system consists of a DFPMSG and back-to-back converter set sized for half of the rated power of the generator. The pros and cons of the system have been stated in terms of cost, efficiency, and fault tolerance, etc. The machine specifications are determined as described by including the aerodynamic behavior of the wind turbine and preexisting wind data. The drawbacks of direct grid connection are minimized by considering the reactive power and optimization pole number according to the wind data during the design stage. The designed control algorithm enables wind power to be shared between the winding sets. This capability could also enable other control schemes, such as thermal management and online maximum efficiency tracking. The proposed concept and control algorithm are verified through experimental studies. The efficiency increase provided by the directly grid-connected winding set would be higher in small-scale WECS applications where converter efficiencies are low. Moreover, the modularity of both the machine and converter can be applied easily to the proposed system.

ACKNOWLEDGMENT

The authors are grateful to the Ege University Planning and Monitoring Coordination of Organizational Development and Directorate of Library and Documentation for their support in editing and proofreading service of this study.

REFERENCES

[1] R. Hemmati, S. Vahid, and A. EL-Refaie, "A novel design for a high specific power interior permanent magnet machine for aerospace applications," in *Proc. IEEE Energy Convers. Congr. Expos. (ECCE)*, Oct. 2020, pp. 1735–1742.

[2] S. Vahid and A. EL-Refaie, "A novel topology for an extendable isolated DC-DC multi-port power converter with a multipurpose hybrid energy storage system," in *Proc. IEEE Energy Convers. Congr. Expo. (ECCE)*, Oct. 2020, pp. 1259–1266.

[3] R. Hemmati, S. Vahid, and A. EL-Refaie, "Comparison of designs utilizing dual phase magnetic material in high specific power electrical machines for aerospace applications," in *Proc. Int. Conf. Electr. Mach. (ICEM)*, vol. 1, Aug. 2020, pp. 2399–2405.

[4] S. Vahid and A. El-Refaie, "Generalized systematic approach applied to design a novel three-port power converter," in *Proc. IEEE Int. Conf. Ind. Technol. (ICIT)*, Feb. 2020, pp. 542–548.

[5] C. Gu, H. Yan, J. Yang, G. Sala, D. D. Gaetano, X. Wang, A. Galassini, M. Degano, X. Zhang, and G. Buticchi, "A multiport power conversion system for the more electric aircraft," *IEEE Trans. Transport. Electrific.*, vol. 6, no. 4, pp. 1707–1720, Dec. 2020.

[6] W. Ding, "Comparative study on dual-channel switched reluctance generator performances under single- and dual-channel operation modes," *IEEE Trans. Energy Convers.*, vol. 27, no. 3, pp. 680–688, Sep. 2012.

[7] M. Korkosz, P. Bogusz, and J. Prokop, "Modelling and experimental research of fault-tolerant dual-channel brushless DC motor," *IET Electr. Power Appl.*, vol. 12, no. 6, pp. 787–796, Jul. 2018.

[8] M. Tezcan, E. Mese, I. Ustoglu, and M. Ayaz, "Analytical modeling of dual winding surface-mounted permanent magnet synchronous machine for hybrid electric vehicle accessory drive systems," *Electr. Power Compon. Syst.*, vol. 45, no. 12, pp. 1353–1369, Jul. 2017.

[9] E. Mese, M. Ayaz, M. Tezcan, and K. Yilmaz, "Design of dual winding permanent magnet synchronous machines for hybrid electric vehicle accessory drives," *Int. J. Vehicle Design*, vol. 69, nos. 1–4, pp. 185–207, 2015.

[10] H. Li and Z. Chen, "Overview of different wind generator systems and their comparisons," *IET Renew. Power Generat.*, vol. 2, no. 2, pp. 123–138, 2008.

[11] V. Yaramasu, B. Wu, P. C. Sen, S. Kouro, and M. Narimani, "High-power wind energy conversion systems: State-of-the-art and emerging technologies," *Proc. IEEE*, vol. 103, no. 5, pp. 740–788, May 2015.

[12] S. Müller, M. Deicke, and R. W. D. Doncker, "Doubly fed induction generator systems for wind turbines," *IEEE Ind. Appl. Mag.*, vol. 8, no. 3, pp. 26–33, May/Jun. 2002.

[13] J. A. Baroudi, V. Dinavahi, and A. M. Knight, "A review of power converter topologies for wind generators," *Renew. Energy*, vol. 32, no. 14, pp. 2369–2385, Nov. 2007.

[14] F. Lydall, "Improvement in polyphase induction motors," British Patent 16 839, Jul. 1902.

[15] L. J. Hunt, "The 'cascade' induction motor," *J. Soc. Telegraph Eng., Including Original Commun. Telegraphy Electr. Sci.*, vol. 52, p. 406, Mar. 1914.

[16] C. S. Brune, R. Spee, and A. K. Wallace, "Experimental evaluation of a variable-speed, doubly-fed wind-power generation system," *IEEE Trans. Ind. Appl.*, vol. 30, no. 3, pp. 648–655, May 1994.

[17] R. A. McMahon, P. C. Roberts, X. Wang, and P. J. Tavner, "Performance of BDFM as generator and motor," *Proc. Inst. Elect. Eng.-Elect. Power Appl.*, vol. 153, no. 2, pp. 289–299, Mar. 2006.

[18] Y. Liu, W. Ai, B. Chen, K. Chen, and G. Luo, "Control design and experimental verification of the brushless doubly-fed machine for standalone power generation applications," *IET Electr. Power Appl.*, vol. 10, no. 1, pp. 25–35, Jan. 2016.

[19] Y. Liu, W. Xu, J. Zhu, and F. Blaabjerg, "Sensorless control of standalone brushless doubly fed induction generator feeding unbalanced loads in a ship shaft power generation system," *IEEE Trans. Ind. Electron.*, vol. 66, no. 1, pp. 739–749, Jan. 2019.

[20] A. Oraee, R. Mcmahon, E. Abdi, S. Abdi, and S. Ademi, "Influence of pole-pair combinations on the characteristics of the brushless doubly fed induction generator," *IEEE Trans. Energy Convers.*, vol. 35, no. 3, pp. 1151–1159, Sep. 2020.

[21] H. Polinder, F. F. A. van der Pijl, G.-J. de Vilder, and P. J. Tavner, "Comparison of direct-drive and geared generator concepts for wind turbines," *IEEE Trans. Energy Convers.*, vol. 21, no. 3, pp. 725–733, Sep. 2006.

[22] D. Bang, H. Polinder, G. Shrestha, and J. A. Ferreira, "Review of generator systems for direct-drive wind turbines," in *Proc. Eur. Wind Energy Conf. Exhib.*, Brussels, Belgium, vol. 31, 2008, pp. 1–11.

[23] F. Blaabjerg, M. Liserre, and K. Ma, "Power electronics converters for wind turbine systems," *IEEE Trans. Ind. Appl.*, vol. 48, no. 2, pp. 708–719, Mar./Apr. 2011.

[24] E. Feilberg, "Investigation of the doubly fed permanent magnet synchronous machine," M.S. thesis, Dept. Elect. Power Eng., Institutt for elkraftteknikk, Halden, Norway, 2009.
[25] A. Stock, J. Teigelkötter, S. Staudt, and T. Kowalski, "The doubly fed permanent magnet synchronous machine as a highly efficient drive system for constant speed applications," in *Proc. IEEE 11th Int. Conf. Power Electron. Drive Syst.*, Jun. 2015, pp. 620–625.
[26] A. J. Thomas, "A doubly-fed permanent magnet generator for wind turbines," Ph.D. dissertation, Dept. Elect. Eng. Comput. Sci., Massachusetts Inst. Technol., Cambridge, MA, USA, 2004.
[27] B. Lu, "Experimental verification for the design of a doubly-fed permanent magnetic generator," Ph.D. dissertation, Dept. Elect. Eng. Comput. Sci., Massachusetts Inst. Technol., Cambridge, MA, USA, 2007.
[28] S. K. Reddy, "Operational behavior of a double-fed permanent magnet generator for wind turbines," Ph.D. dissertation, Dept. Elect. Eng. Comput. Sci., Massachusetts Inst. Technol., Cambridge, MA, USA, 2005.
[29] Z. Zhang, "A brushless doubly fed machine with separated field and armature windings in dual stators," in *Proc. IEEE Int. Electr. Mach. Drives Conf. (IEMDC)*, May 2019, pp. 295–300.
[30] E. Meşe, A. Bakbak, M. Ayaz, M. Boztepe, M. Altıntaş, O. Akın, and H. T. Canseven, "Development of doubly-fed direct drive modular permanent magnet wind generator," in *Proc. 8th Int. Conf. Renew. Energy Res. Appl. (ICRERA)*, Nov. 2019, pp. 864–868.
[31] E. Mese, M. Tezcan, M. Ayaz, Y. Yasa, and K. Yilmaz, "Design considerations for dual winding permanent magnet synchronous machines," in *Proc. IEEE Energy Convers. Congr. Expo. (ECCE)*, Sep. 2012, pp. 1894–1901.
[32] P. C. Krause, O. Wasynczuk, S. D. Sudhoff, and S. Pekarek, *Analysis of Electric Machinery and Drive Systems*, vol. 2. Hoboken, NJ, USA: Wiley, 2002.
[33] K. Ogata, *Modern Control Engineering*. Upper Saddle River, NJ, USA: Prentice-Hall, 2010.
[34] P. Han, M. Cheng, and R. Luo, "Design and analysis of a brushless doubly-fed induction machine with dual-stator structure," *IEEE Trans. Energy Conv.*, vol. 31, no. 3, pp. 1132–1141, Sep. 2016.
[35] T. D. Strous, X. Wang, H. Polinder, and J. A. B. Ferreira, "Brushless doubly-fed induction machines: Torque ripple," in *Proc. IEEE Int. Electric Mach. Drives Conf. (IEMDC)*, May 2015, pp. 1145–1151.
[36] S. Abdi, E. Abdi, and R. McMahon, "A study of unbalanced magnetic pull in brushless doubly fed machines," *IEEE Trans. Energy Convers.*, vol. 30, no. 3, pp. 1218–1227, Sep. 2015.
[37] T. D. Strous, H. Polinder, and J. A. Ferreira, "Brushless doubly-fed induction machines for wind turbines: Developments and research challenges," *IET Elect. Power Appl.*, vol. 11, no. 6, pp. 991–1000, Jul. 2017.
[38] H. Polinder, "Overview of and trends in wind turbine generator systems," in *Proc. IEEE Power Energy Soc. Gen. Meeting*, Jul. 2011, pp. 1–8.
[39] A. M. El-Refaie, "Fractional-slot concentrated-windings synchronous permanent magnet machines: Opportunities and challenges," *IEEE Trans. Ind. Electron.*, vol. 57, no. 1, pp. 107–121, Jan. 2010.
[40] T. D. Strous, U. Shipurkar, H. Polinder, and J. A. Ferreira, "Comparing the brushless DFIM to other generator systems for wind turbine drive-trains," *J. Phys., Conf. Ser.*, vol. 753, no. 11, Sep. 2016, Art. no. 112014.
[41] J. Carroll, A. McDonald, D. McMillan, T. Stehly, C. Mone, and B. Maples, "Cost of energy for offshore wind turbines with different drive train types," in *Proc. EWEA Annu. Event*, 2015, pp. 1–9.
[42] J. F. Manwell, J. G. McGowan, and A. L. Rogers, *Wind Energy Explained: Theory, Design and Application*. Hoboken, NJ, USA: Wiley, 2010.
[43] T. Ackermann, *Wind Power in Power Systems*. Hoboken, NJ, USA: Wiley, 2005.
[44] H. Rinne, *The Weibull Distribution: A Handbook*. Boca Raton, FL, USA: CRC Press, 2008.
[45] U. Eminoglu and S. Ayasun, "Modeling and design optimization of variable-speed wind turbine systems," *Energies*, vol. 7, no. 1, pp. 402–419, Jan. 2014.
[46] M. Çubukçu and A. Özdamar, "Enerji eldesinde ortalama rüzgar hizi ölçüm araliği ve Hellman katsayisinin önemi: Söke örneği," in *Proc. 2nd Yenilenebilir Enerji Kaynaklari Sempozyumu Bildiriler Kitabi*, 2003, pp. 211–218.
[47] J. Wang, X. Huang, Q. Li, and X. Ma, "Comparison of seven methods for determining the optimal statistical distribution parameters: A case study of wind energy assessment in the large-scale wind farms of China," *Energy*, vol. 164, pp. 432–448, Dec. 2018.
[48] N. Bianchi and M. D. Prè, "Use of the star of slots in designing fractional-slot single-layer synchronous motors," *IEE Proc.-Electr. Power Appl.*, vol. 153, no. 3, pp. 459–466, May 2006.
[49] Z. Q. Zhu, M. L. M. Jamil, and L. J. Wu, "Influence of slot and pole number combinations on unbalanced magnetic force in PM machines with diametrically asymmetric windings," *IEEE Trans. Ind. Appl.*, vol. 49, no. 1, pp. 19–30, Jan./Feb. 2013.
[50] N. Bianchi, S. Bolognani, M. D. Pré, and G. Grezzani, "Design considerations for fractional-slot winding configurations of synchronous machines," *IEEE Trans. Ind. Appl.*, vol. 42, no. 4, pp. 997–1006, Jul./Aug. 2006.
[51] A. M. El-Refaie, T. M. Jahns, and D. W. Novotny, "Analysis of surface permanent magnet machines with fractional-slot concentrated windings," *IEEE Trans. Energy Convers.*, vol. 21, no. 1, pp. 34–43, Mar. 2006.
[52] J. L. Kirtley, *Electric Power Principles: Sources, Conversion, Distribution and Use*. Hoboken, NJ, USA: Wiley, 2020.
[53] M. Ayaz, A. Bakbak, H. T. Canseven, M. Altintas, E. Mese, O. Akin, and M. Boztepe, "Design considerations on E-core for modular and scalable permanent magnet synchronous machine," in *Proc. 6th Int. Conf. Electr. Power Energy Convers. Syst. (EPECS)*, Oct. 2020, pp. 141–145.

ALI BAKBAK received the B.Sc. degree (Hons.) from Niğde University, Niğde, Turkey, in 2012, and the M.Sc. degree from Celal Bayar University, Manisa, Turkey, in 2016, and the Ph.D. degree from Ege University, İzmir, Turkey, in 2021, all in electrical and electronics engineering. His research interests include modeling, design, and control of electrical machines.

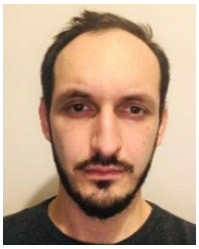

MERT ALTINTAS received the bachelor's degree, in 2015, and the master's degree from the Department of Electrical and Electronics Engineering, Ege University, in 2018, where he is currently pursuing the Ph.D. degree. He is currently working as a Research Assistant with the Electrical and Electronics Engineering Department, Ege University. His research interests include power electronics and control of electric machine systems.

MURAT AYAZ received the B.S., M.S., and Ph.D. degrees from the Department of Electrical Education, Kocaeli University, Kocaeli, Turkey, in 2005, 2008, and 2015, respectively. Between 2005 and 2009, he worked as a Project Engineer with Beck & Pollitzer, Kocaeli. From 2009 to 2015, he was worked as a Research Assistant with the Electrical Education Department, Kocaeli University, where he is currently an Assistant Professor with the Electric and Energy Department. He has several studies on electric machine design and industrial automation system design. His research interests include electric machines, electromechanical systems, hybrid electric vehicles, and industrial automation systems.

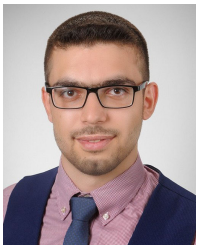

HUSEYIN TAYYER CANSEVEN received the B.Sc. degree from the Department of Electrical and Electronics Engineering, Ege University, İzmir, Turkey, in 2018, where he is currently pursuing the M.Sc. degree in electrical and electronics engineering. He is currently a Research Assistant with the Department of Electrical and Electronics Engineering, Kütahya Dumlupınar University, Kütahya, Turkey. His research interests include electrical machine modeling and wind energy conversion systems.

MUTLU BOZTEPE (Member, IEEE) received the B.Sc. degree from Dokuz Eylül University, İzmir, Turkey, in 1991, and the M.Sc. and Ph.D. degrees from Ege University, İzmir, in 1995 and 2002, respectively. He is currently an Associate Professor with the Department of Electrical and Electronics Engineering, Ege University. His research interests include power electronics, design and control of power converters, and grid integration of photovoltaic systems.

OZKAN AKIN received the B.Sc. degree in electrical engineering from Kocaeli University, Kocaeli, Turkey, in 2002, and the M.Sc. and Ph.D. degrees in electrical engineering from Ege University, İzmir, Turkey, in 2006 and 2013, respectively. He is currently an Assistant Professor with the Department of Electrical and Electronics Engineering, Ege University. His research interests include electrical machine control, digital electronics, power electronics, and real-time digital simulation and control.

ERKAN MESE (Member, IEEE) received the B.Sc. and M.Sc. degrees in electrical engineering from Istanbul Technical University, Istanbul, Turkey, in 1990 and 1993, respectively, and the Ph.D. degree in electrical power engineering from Rensselaer Polytechnic Institute, Troy, NY, USA, in 1999. He worked in various positions in the industry, including Advanced Energy Conversion, General Motors, AVL. As of 2009, he started to serve as a Faculty Member with the Electrical Engineering Department, Yildiz Technical University. Since 2016, his faculty membership continues with the Department of Electrical Engineering and Electronics Engineering, Ege University, İzmir, Turkey. His research interests include electrical machines, electromechanical systems, power electronics, hybrid electric vehicles, and renewable energy systems.